Article:

Rosado Hau, N., Ma, L. orcid.org/0000-0002-3731-8464, Ingham, D. et al. (1 more author) (2020) A critical analysis of the stall onset in vertical axis wind turbines. Journal of Wind Engineering and Industrial Aerodynamics, 204. 104264. ISSN 0167-6105

https://doi.org/10.1016/j.jweia.2020.104264

A critical analysis of the stall onset in vertical axis wind turbines

Nidiana Rosado Hau[a,b], Lin Ma[a], Derek Ingham[a], Mohamed Pourkashanian[a]

[a] *Energy 2050, University of Sheffield, United Kingdom, S10 2TN*
[b] *Facultad de Ingenieria, Universidad Autonoma de Yucatan*

Abstract

The dynamic stall phenomenon in Vertical Axis Wind Turbines (VAWTs) appears, under some operating conditions, to be not very well defined, such as at a low tip speed ratio. Some studies have focused on describing the topology of the dynamic stall but little attention has been paid to understand how all the operating VAWT parameters influence the moment of stall inception. This paper focuses on analysing the influence of the tip speed ratio, pitch angle, reduced frequency, relative velocity and Reynolds number on the stall-onset angle of VAWTs. CFD simulations with an oscillating NACA0015 describing the angle of attack and relative velocity in VAWTs were employed. The results have revealed that an increase in the stall-onset occurs anytime the operating parameters increase the value of the non-dimensional pitch rate and the Reynolds number at the moment the angle of attack approaches to the static stall angle. The stall-onset angle showed a linear increase with the non-dimensional pitch rate in the range of Reynolds number tested, namely $0.8 - 3.3 \times 10^5$. This paper has elucidated how the several parameters governing VAWTs operation effect the stall-onset angle and therefore has contributed to a much better understanding of the causes that induce the stall in these devices.

Keywords:
Vertical axis wind turbine, Stall-onset, Dynamic stall, Reduced frequency, Reynolds number, Pitch angle

1. Introduction

Vertical Axis Wind Turbines (VAWTs) have drawn much attention of research and industry due to their potential to be installed in urban and offshore regions, and in particular where the wind resource

Email address: nidiana.rosado@correo.uady.mx (Nidiana Rosado Hau)

Nomenclature

C	Constant variable
C_C, C_D, C_L	Chordwise, drag and lift force coefficients
C_{fx}	Skin friction, $\sigma_x/0.5\rho U_{ref}^2$
C_p	Pressure coefficient
D	Rotor diameter, m
L, M	Lift stall and moment stall points
R	Rotor radius, m
T	Period of oscillation
U	Incoming wind flow for the oscillating aerofoil, m/s
U_{ref}	Actual wind speed, m/s
V_∞	Free stream wind velocity in the VAWTs, m/s
V_{inst}	Wind sped at a specific time, m/s
V_{mean}	Average of the relative velocity in one revolution, m/s
V_{rel}	Relative velocity, m/s
c	Chord, m
q	Non-dimensional pitch rate
t	Time, s
x/c	Non-dimensional chord distance
$\alpha(t)$	Angle of attack, (°)
α_{max}	Maximum angle of attack in the upstroke
α_{os}	Dynamic stall-onset angle, (°)
α_{ss}	Static stall angle, (°)
$\dot{\alpha}$	Pitch rate, (rad/s)
β	Pitch angle, (°)
κ	Reduced frequency, $(\omega c/2U_{ref})$
λ	Tip speed ratio, $\omega R/V_\infty$
ω	Rotational speed, rad/s

presents highly variable wind speed and direction [1]. In order to understand its aerodynamics, many authors have used URANS Computational Fluid Dynamics (CFD) simulations to explore qualitatively the influence of the aerofoil profile [2, 3, 4, 5], the pitch angle [6, 7, 8], Reynolds number [9, 10, 11, 12] and the number of blades [1, 13, 7, 14] on the power coefficient.

The aerodynamic investigations on VAWTs have confirmed that the presence of the dynamic stall phenomenon has been observed under some operating conditions and still it is not very well known except that it is being associated mainly to low tip speed ratios (TSRs). The range of TSRs where dynamic stall appears has been found to be different in each case investigated [15, 16, 17, 18, 19, 20, 21]. In addition, the parameter c/D, that relates the chord length and diameter, have been demonstrated to play a significant role in the development of dynamic stall on VAWTs and according to Buchner et al. [22], the tip speed ratio alone is not sufficient to describe the dynamic stall phenomenon.

In the VAWT, when dynamic stall takes place then this degrades its power coefficient and induces high structural loads on the rotor [23]. The vortex formation and its release to the wake characterizes the dynamic stall on VAWTs. If the dynamic stall is severe, multiple vortices are released, and an additional decrease in the power coefficient is observed [24]. The generation of the vortices has been observed to be more prominent in the upstream section of the rotor but may appear downstream of the rotor [25, 16].

In order to improve the VAWTs performance and to regulate the dynamic stall that induces the undesired unsteady loads, it is fundamental to determine the operating and physical conditions that control the stall-onset in the upstream region of the VAWTs. Since previous studies have investigated mostly the impact of the tip speed ratio, the present analysis addresses the need in understanding the influence on the stall-inception of the several parameters governing VAWTs operation.

The stall-onset angle (α_{os}), represents the inception of the stalling process. Under static conditions, this angle is recognizable by the angle where a sudden loss in the lift occurs but under dynamic conditions, this is not the case [26] and attention to other aerodynamic characteristics need to be made. Under dynamic conditions, stall inception occurs immediately after a laminar bubble, that is concentrated near the aerofoil leading edge (LE), experiences a maximum in the pressure coefficient (negative), then, a vortex is initiated and detaches from the LE [27, 28] and the presence of the vortex affects the unsteady aerodynamic forces.

An example of the unsteady aerodynamic forces under dynamic stall for oscillating aerofoils is shown in Fig.1. At the stall-onset, the lift coefficient (C_L) starts to deviate from its linear attached trend and increases in value (over-lift) due to the movement of the vortex downstream along the chord; the lift coefficient reaches its maximum value when the vortex is located at the mid chord position and then, stalls, this point is called lift stall (L). In addition, a deviation occurs in the drag force coefficient (C_D) and the pitching moment coefficient (C_M). Further, McAlister, [29] has suggested that the maximum chordwise force coefficient, (C_c), is the point that is a more quantifiable criterion to select for the stall-onset angle. A discussion of different techniques to define the stall-onset angle is found in [30, 31].

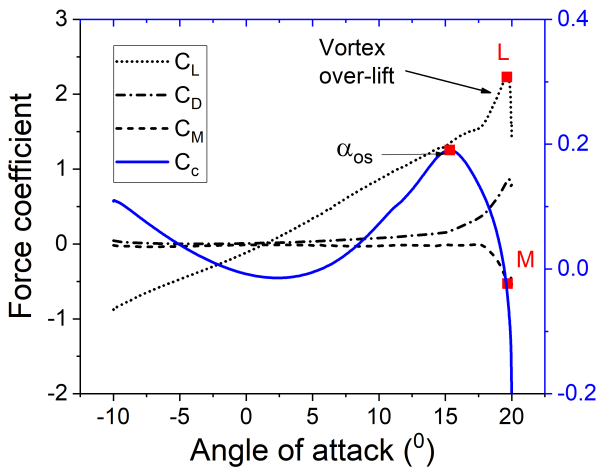

Figure 1: A typical unsteady loads coefficient as a function of the angle of attack that illustrates the lift stall point (L), moment stall (M) and stall-onset angle (α_{os}).

The stall-onset angle is a critical parameter in describing the dynamic stall process since it marks the inception of the leading edge vortex. Thus, the larger is the stall-onset angle then the later the vortex formation and the severity of the stall conditions may be reduced. For example, the point where the sudden loss in the lift force occurs is moved to a larger angle of attack as well as the point where a large negative pitching moment is observed [32]. In addition, the large hysteresis in the unsteady loads due to the presence of the vortex decreases, and the stall conditions change from deep stall to light stall or even non-stall conditions. Therefore, investigating how the operating conditions affect the stall-onset angle is an essential task in improving the aerodynamics and the design of the VAWTs.

There is a large amount of experimental and numerical investigation on the dynamic stall phenomenon [32, 33, 34, 35, 36, 37]. The ramp-up tests, that have a constant pitch rate $\dot{\alpha} = C$, have demonstrated this parameter as being the most crucial parameter [38, 39, 40, 41, 42, 43, 44] to define the stall-onset. In oscillating motions, where the pitch rate is a function given by $\dot{\alpha} = f(t)$, the variables that affect the inception point are less clear, since the amplitude and mean angle of oscillation and reduced frequency affect the angle of attack equation and hence the pitch rate function [29, 30, 45, 46].

Sheng et al. [30] evaluated the stall-onset angle of several oscillating aerofoils, and they proposed similarly to the ramp-up tests a non-dimensional parameter called the equivalent reduced pitch rate that is the product of the amplitude and the reduced frequency. This equivalent reduced pitch rate was shown to be the most crucial parameter that defines the stall-onset in the oscillating motion. The same equivalent reduced pitch rate was used in [47] and a similar linear trend between the equivalent reduced pitch rate and the stall-onset angle was found. More recently, Mulleners et al. [31] experimentally found for oscillating aerofoils that the non-dimensional pitch rate at the static-stall angle was the parameter that is the most critical factor in determining the stall-onset and the previous proposed equivalent reduced pitch rate in [30] did not show a clear relation with the stall-onset.

In the VAWTs, the number of operating conditions that may affect the stall-onset angle is larger compared with the ramp-up and sine-pitching motions. For example, the stall-onset can be affected by the tip speed ratio, pitch angle, rotational speed, Reynolds number and the constantly changing relative velocity. Thus, despite the efforts made by several authors, defining how these operating parameters affect the stall-onset angle results in a very complicated task when using a full wind turbine [22].

This paper uses a systematic methodology to understand how the mentioned variables affect the stall-onset angle and the dynamic stall in VAWTs. First, an analysis of the tip speed ratio, reduced frequency and pitch angle at a constant Reynold number is performed by using CFD simulations of an oscillating NACA0015 describing the angle of attack of a VAWT. Second, the relation among all the mentioned variables with the non-dimensional pitch rate parameter and their effect on the stall-onset angle is elucidated. Finally, the effect of the relative velocity is investigated by using the oscillating NACA0015 aerofoil with a time-varying incoming flow.

This paper is divided as follows: In Section 2, the operating parameters employed in the simulations are defined and the methodology to calculate the stall-onset angle is described respectively; Section 3 describes the numerical techniques employed. Section 4 describes the effect of the TSR, pitch angle, reduced frequency, Reynolds number, Variable wind speed at the stall-onset angle of the VAWTs, and Section 5 discusses the present findings and their application in VAWTs; Finally, conclusions are included in Section 6.

2. Methodology

2.1. Description of the operating parameters

In this paper, two-dimensional CFD simulations that agree very well with the experimental data were employed. The description of the numerical strategy is included in Section 3. In order to evaluate the effect of the operating conditions on the stall-onset angle, then two approaches were used.

First, an incoming wind flow U with a constant magnitude (depending on the chord-based Reynolds number under evaluation) past an oscillating aerofoil, as illustrated in Fig. 2. The oscillating aerofoil describes a motion with the angle of attack $\alpha(t)$ for a VAWTs [23] given as follow:

$$\alpha(t) = \arctan(\frac{\sin(\omega t)}{\lambda + \cos(\omega t)}) - \beta \tag{1}$$

where, λ is the tip speed ratio; ω is the rotational speed; t is the time and, β is the pitch angle. β is positive outwards from the circle described by the outer edge of the rotation of a VAWT blade. For this oscillating aerofoil β positive is indicated in Fig. 2. The angle of attack represents the angle between the aerofoil-chord and the incoming wind flow U aligned all the time to the x-axis.

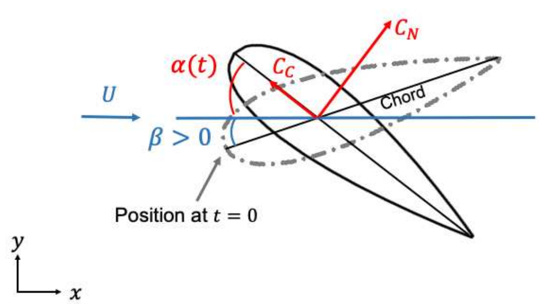

Figure 2: Sketch of an oscillating aerofoil with the VAWT angle of attack $\alpha(t)$ and an incoming flow (U). U can take a constant magnitude or a time-varying magnitude given by the relative velocity equation.

The value of ωt from 0 to π represents the upstream zone of the rotor, and from π to 2π the downstream zone. Positive angles of attack are associated with the upstream zone of the rotor and negative angles with the downstream zone.

In order to replicate the angle of attack motion given by Eq. (1) in the CFD simulations, a user defined function (UDF) was employed to control the pitching rate of the rotating mesh domain (mesh domain explained in Section 3.1.2) according to the equation:

$$\dot{\alpha}(t) = \omega \frac{(1 + \lambda \cos{(\omega t)})}{(1 + 2\lambda \cos(\omega t) + \lambda^2)} \tag{2}$$

(i) Using this first approach, at a constant Reynolds number the influence of the tip speed ratio (λ), pitch angle (β) and the angular velocity (ω) that affect the angle of attack given in Eq. (1) were investigated. The rotational speed was expressed in terms of the non-dimensional parameter, called the reduced frequency (κ) as $\omega = 2\kappa U_{ref}/c$. U_{ref} represents the actual wind speed that impacts the aerofoil. For this first approach, with an incoming wind flow with a constant magnitude, $U = U_{ref}$ and takes a value of 20 m/s to obtain a Reynolds number base on the chord-aerofoil of 2×10^5.

The tip speed ratios investigated were 2 and 3 as these are typically found to be small enough to allow the presence of dynamic stall in VAWTs. Additionally, the values of κ tested are in the range of the average reduced frequency ($c/2R$), between 0.025 and 0.1828, as found in VAWTs [13, 48, 49].

(ii) The non-dimensional pitch rate parameter, q, that is formulated by Daley et al. [44] is given as:

$$q = \dot{\alpha}c/(2U_{ref}) \tag{3}$$

It is necessary to emphasize that the pitch rate $\dot{\alpha}$ and the velocity changes constantly in VAWTs, thus, the non-dimensional pitch rate q uses the values of the pitch rate and the relative velocity at a specific time, t, as input values corresponding to $\dot{\alpha}$ and U_{ref} respectively. The expression in Eq.(3) is also used to calculate the non-dimensional pitch rate in the ramp-up motion, but because the pitch rate $\dot{\alpha}$ has a constant value then q is easily calculated.

In the second approach, the incoming wind flow U, as represented in Fig. 2, was a time-depend function given by the relative velocity equation of VAWTs as follows:

$$V_{rel} = V_{\infty} \sqrt{1 + 2\lambda \cos(\omega t) + \lambda^2} \tag{4}$$

where, V_{∞} represents the incoming free-stream wind velocity on the VAWT rotor.

For this approach, a user defined function was implemented to vary the incoming flow (inlet velocity) according to Eq.(4) and at the same time the pithing rate according to Eq. (2). In order to have a single value of the non-dimensional pitch rate using Eq. (3) then, the pitch rate, $\dot{\alpha}$ and U_{ref} uses the value of the Eq. (2) and Eq. (4), respectively, at the instant of time t when the angle of attack approaches the static stall angle.

(iii) The constantly changing relative velocity described by the Eq. (4), has been investigated in order to assess its influence on the stall-onset and to compared the existing difference on the stall-onset angle when using a constant-average relative velocity. The average relative velocity, ωR or λV_∞, that is an approximated average of the Eq. (4) in one revolution, is typically used in VAWTs in order to simplify the analysis [17, 50]. Thus, it is interesting to investigate if a difference exists when using the actual relative velocity rather than its average value.

2.2. Stall-onset estimation

As mentioned previously, there are several techniques to identify the stall-onset angle. In this paper, the stall-onset angle, α_{os}, is calculated as the angle where a maximum value in the chordwise force coefficient is observed. This criterion is also recommended in [29, 34, 51].

The chordwise force coefficient, C_c, for an oscillating aerofoil is represented in Fig. 2 and is described as follows:

$$C_c = C_L \sin(\alpha) - C_D \cos(\alpha) \tag{5}$$

Due to the prominent influence of the dynamic stall in the upstream zone of the VAWT, [25, 16], i.e. from $\omega t = 0 - \pi$, in this paper we focus on evaluating the stall-onset angle in this range of angle of attack.

3. Computational fluid dynamic simulations

3.1. Unsteady simulations

The two-dimensional URANS simulations used in this investigation were validated very carefully with the available experimental data of an oscillating NACA0012 aerofoil. The Reynolds number for this data is 1.35×10^5 (chord-based); the aerofoil chord-length, $c = 15$ cm; the reduced frequency $\kappa = 0.1$, and the intensity of the turbulence was 0.08 %, similar to the experimental conditions of the wind tunnel test case [37]. This experimental data is selected since VAWTs for urban environments can experience a Reynolds number as low as 1×10^5 [10, 14] and this is the main interest of the present study.

Several numerical investigations of the selected experimental data in [37] have been performed in order to determine a numerical strategy that considers the mesh, time and domain independence analysis for oscillating aerofoils at low Reynolds numbers [46, 52, 53, 54]. This is beneficial to verified the numerical techniques performed in this paper.

3.1.1. Numerical settings

In the present simulations, the turbulent transitional model $\kappa\omega - SST - \gamma$ was selected due to the Reynolds number being studied, namely $0.8 - 3.3 \times 10^5$, where the boundary layer flow transition is likely to occur and a transitional model is recommended at such Reynolds numbers [55, 56, 57]. A discussion of the influence of the turbulence models of this experimental case has been made in [57] and the use of a transitional model is recommended.

The COUPLED method that is a non-segregate method of pressure coupling with an implicit scheme was selected due to the advantages of fast convergence for coarse meshes and coarse time steps as described in ANSYS FLUENT 17.2. Additionally, the COUPLED method has the capabilities of detecting divergence and automatically reduces the Courant Number (CFL). The default CFL is 200 and a reduction to 10-50 is recommended if there are difficulties with convergence, thus a CFL=10 was selected. A full convergence criterion with a relative residual less than 1×10^{-5} was used with 100 iterations per time step. At least four oscillating cycles were run for each simulation before collecting the results, and in most cases, a convergence in the lift force coefficient was achieved after the second cycle. This agrees with the statistical convergence observed by Geng. et al. [57]. A second-order discretization (spatial and temporal) and a hybrid initialization was set up in all the simulations.

3.1.2. Mesh domain and boundary conditions

The mesh topology consist of two domains: a rotating domain with an unstructured mesh shows in Fig 3(a) and, a stationary domain consisting of a structured mesh, Fig. 3(b).

In the experimental data, a closed wind tunnel was used with the walls allocated to be three times the chord-length of the aerofoil from the centre of the pitching motion. Thus, to be consistent with the experimental test conditions, non-slip conditions were applied for the upper and lower bounds of the domain with an original distance of 3 times the chord-length. Moreover, due to the interest in studying aerofoils in an open environment, then the distance of the upper and lower boundaries from the pitching position of the aerofoils (1/4 c) was increased to 3, 10, 15 and 20 times the characteristic length, c, in order to find a domain with no influence on the forces on the aerofoil. The influence of this distance is observed in the resulting lift coefficient and very similar results were obtained using

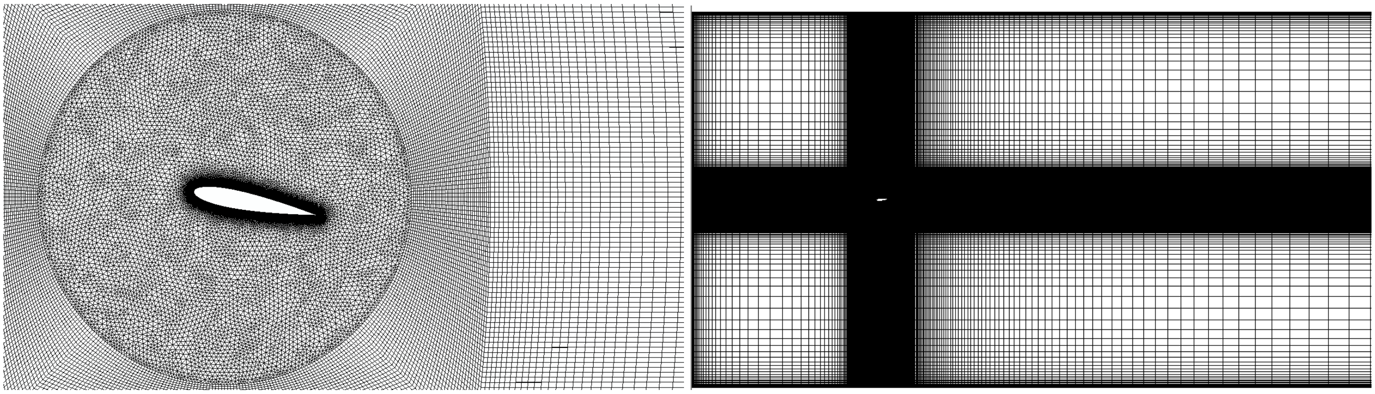

(a) (b)

Figure 3: Mesh topology (a) around the aerofoil with 1000 nodes, and (b) for the non-rotational region with the final settings of the domain.

distances of 10, 15 and 20 c. Therefore, $15c$ was selected as the distance from the pitching point to the boundaries (lower and upper), and this was enough to avoid the influence of the upper and lower boundaries. The pressure outlet was set to be $45c$ from the pitching point of the oscillating aerofoil, and the velocity inlet was set to be $15c$ from the oscillating point. Both distances are considered to be large enough to allow the development of the wake and within the recommendations of several investigations [52, 54].

The aerofoil profile was set as non-slip conditions and due to the importance of solving the viscous layer, then 60 layers were collocated around the aerofoil and the y+ in the boundary layer was less than 1.2.

A mesh independence analysis with four grids with the parameters as given in Table 1 was performed. The number of nodes around the aerofoil investigated was 500, 1000, 2000 and 4000; however, no large impact was found in the force coefficients observed in Fig. 4(a) within this range of nodes, and therefore 1000 nodes were selected for the final settings.

Table 1: Characteristics of the evaluated meshes.

Parameter	G1	G2	G3	G4
Nodes on aerofoil	500	1000	2000	4000
Total mesh elements	140000	200000	300000	500000

A time step independence study was conducted with a non-dimensional time constant ($\tau = t/T$)

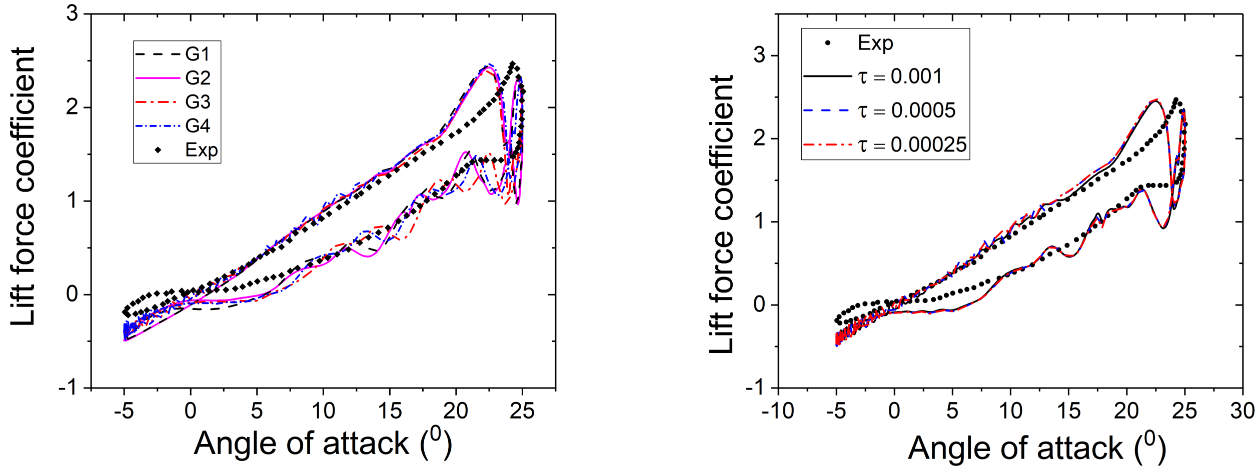

(a) (b)

Figure 4: (a) Mesh independence study, and (b) time step independence study.

of 0.001, 0.0005 and 0.00025. These time steps correspond to a step increment of 0.1, 0.05 and 0.025 degrees in the angle of attack, respectively. Similar results were obtained for the lift force coefficient, as observed in Fig. 4(b), for all the time steps studied and therefore, $\tau = 0.0005$ was selected as the best option.

3.1.3. Numerical verification

The present URANS simulations were validated against the URANS simulation performed by Geng et al. [54], and the Large Eddy Simulations (LES) carried out by Geng et al. [54] and Kim et al. [53], and a comparison among these four simulations is shown in Fig. 5(a). Very good agreement in the prediction of the lift force coefficient, C_L, was observed among present 2D CFD simulations, Geng et.al 2D CFD simulations [54] and Geng et al. LES simulations [54].

For all the numerical simulations, 2D CFD and LES, the linear region of variation of the lift force coefficient with angle of attack is in very good agreement with the experimental data. The deviation in C_L, that appears once the vortex has been released, suggests that the stall-onset angle may be predicted with the same accuracy for all the numerical techniques compared in Fig. 5 (a). Unfortunately, the significant C_L peak observed in the experimental data was not captured by any of the numerical simulations. Since this peak indicates that a vortex is located at the mid-chord of the aerofoil, thus, the accuracy in predicting the stall-onset angle is not affected and this angle is the focus of this paper.

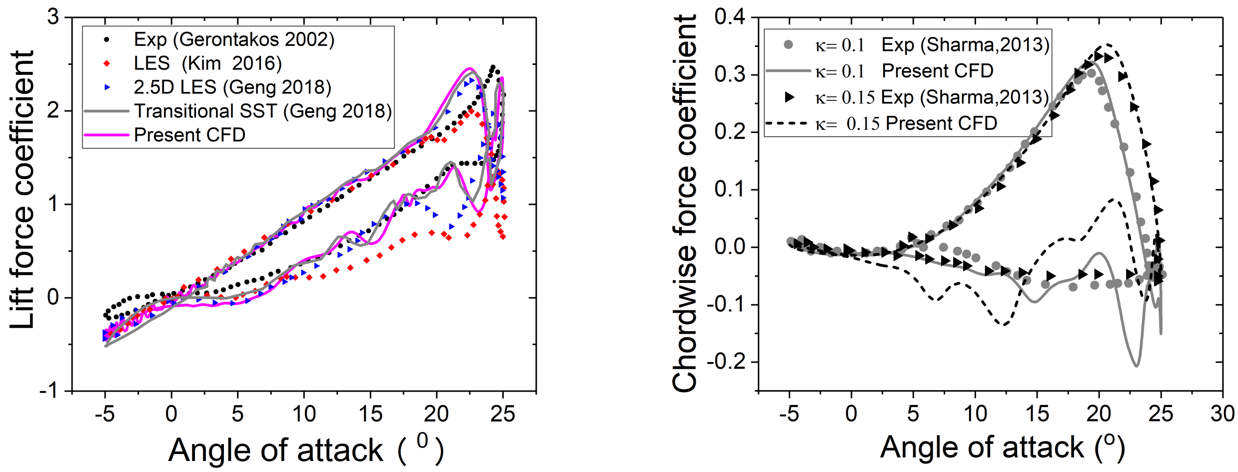

(a) (b)

Figure 5: (a) The lift coefficient as a function of the angle of attack of the aerofoil NACA0012 at Re 1.35×10^5 and the comparison with the experimental data [37]. (b) Chordwise force coefficient of the NACA0015 as a function of the angle of attack with a VAWT motion at Re 2×10^5 [58].

Further, to demonstrate the accuracy of the present numerical methodology to capture the stall-onset angle, a second validation is performed by using the experimental data of a NACA0015 aerofoil that describes the same motion as the previous experimental case, i.e. $\alpha(t) = 10 + 15 \sin \omega t$ at Re 2×10^5. The advantage of this second case results in the available data of the chordwise force coefficient. The numerical predictions of the stall-onset angle are obtained for the reduced frequency values of $\kappa = 0.1$ and $\kappa = 0.15$ and these are included in Fig. 5(b). Excellent agreement was observed in the prediction of the peak in the chordwise force coefficients. Hence, the present numerical simulations, since they capture with an excellent agreement the chordwise force with the experimental data, may be considered accurate enough to investigate the stall-onset angle.

3.2. Static simulation

Due to the interest in evaluating the static stall angle for three Reynolds numbers, namely, 0.8, 2 and 3.3 $\times 10^5$, static simulations were performed by using the same mesh characteristics as those employed in the unsteady simulations. The number of iterations used was 10000 to ensure a full stabilization of the lift force coefficient and then, the static stall angle obtained for each aerofoil was:10°, 13°, 14° for the Reynolds numbers 0.8, 2 and 3.3 $\times 10^5$, respectively. The Reynolds number was changed by varying the incoming flow to 8, 20 and 33 m/s.

4. Results

4.1. Influence of κ, λ and β at constant Reynolds number

The analysis of the influence of the reduced frequency (κ), tip speed ratio (λ) and pitch angle (β) on the stall-onset angle by using the first approach for a constant Reynolds number has shown the following results:

(i) With the increase in the reduced frequency (κ), the calculated stall-onset angle (α_{os}) increases. For example, in the simulation with a reduced frequency of $\kappa = 0.09$, the stall-onset angle was $\alpha_{os} = 20.60°$. Decreasing the reduced frequency to $\kappa = 0.06$ produced the stall-onset angle $\alpha_{os} = 18.79°$. For both values of κ the tip speed ratio was $\lambda = 2$ and the pitch angle was $\beta = -11°$.

The delay in the stall conditions with the increase in the reduced frequency is also observed in the comparison of the pressure coefficient (C_p) and skin friction (C_{fx}) curves including in Fig. 6(a-b). The skin friction at the Reynolds number 2×10^5 for two dynamic cases with reduced frequencies $\kappa = 0.09$ and $\kappa = 0.06$, and one static simulation were computed at the angle of attack of 13°. At the static condition, the aerofoil stalls at 13° and thus a high negative pressure coefficient is observed close to the aerofoil leading edge. This is a critical point where a laminar separation bubble (LSB) concentrated at the LE collapsed [34]. For the unsteady simulations, this high minimum pressure is not reached, suggesting a delay in the pressure collapsed for the reduced frequency $\kappa = 0.06$ and a further delay for the reduced frequency $\kappa = 0.09$.

Another interesting characteristic that confirms the delay in the stall is recognized by observing the skin friction (C_{fx}), as plotted in Fig. 6(b). The closer the laminar separation bubble (LSB) to the aerofoil leading-edge indicates an earlier collapse of the pressure coefficient and, an earlier separation of the boundary layer occurs. The region occupied by the LSB is exemplified for the static case in Fig. 6(b) by circular and triangular symbols; at these two points the skin friction experiences a zero value. The LSB region for the unsteady cases with a reduced frequency $\kappa = 0.06$ is closer to the leading edge of the aerofoil compared for the case with the reduced frequency $\kappa = 0.09$.

Moreover, the point where the turbulent boundary layer (formed after the reattachment of the LSB) experiences $C_{fx} = 0$ is an additional parameter of reference to evaluate the magnitude of the

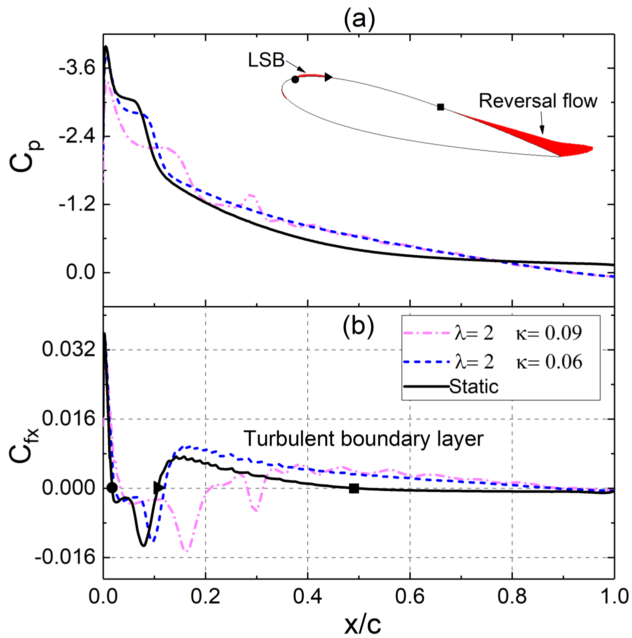

Figure 6: (a) Pressure coefficient, and (b) skin friction along the chord of an oscillating aerofoil at the angle of attack 13°. ● Laminar boundary layer separation, ▶ Reattachment of LSB, ■ Start of reversal flow in the turbulence boundary layer at TE.

delay in the stall-onset angle; closer is this point to the LE, then the sooner stall occurs. For the static case, the turbulent boundary layer experiencies $C_{fx} = 0$ at 50 % of the chord, this point is indicated with a square in Fig 6 (b). For the unsteady cases with $\kappa = 0.06$ and $\kappa = 0.09$ the turbulent boundary layer with $C_{fx} = 0$ is located at 95% and 97 % from the LE. More details on the pressure coefficient and skin friction behaviours under unsteady conditions are described by Ekaterinaris & Platzer [55].

The increase of the stall-onset angle with the reduced frequency is confirmed by comparing the calculated stall-onset angle, α_{os}, for another two dynamic simulations with $\kappa = 0.02$ and $\kappa = 0.04$ using both a tip speed ratio of $\lambda = 3$ and a pitch angle of $\beta = -11°$ at Re 2×10^5. The stall-onset angle, α_{os}, results in 14.70° and 16.22° for the reduced frequencies $\kappa = 0.02$ and 0.04, respectively.

(ii) The influence analysis of the tip speed ratio (λ) has shown that with a decrease in λ the stall-onset angle (α_{os}) grows. For the tip speed ratios investigated with values 2, 2.37 and 3, the computed α_{os} were 18.82°, 17.68° and 16.56°, respectively. The skin friction for these dynamic cases is illustrated in Fig. 7 (a) and it was revealed that the lower is λ then more is the delay in the stall-onset angle.

For example, the position of the laminar bubble (first two locations with $C_{fx} = 0$), is closer to the leading edge aerofoil for $\lambda = 3$, followed by $\lambda = 2.37$ and finally $\lambda = 2$. Moreover, the point where the turbulent boundary layer experiences $C_{fx} = 0$, which indicates the start of reverse flow, is located at 84 % from the aerofoil LE for $\lambda = 3$, at 86 % for $\lambda = 2.37$ and 88% for $\lambda = 2$. Therefore, this indicates that the tip speed ratio $\lambda = 2$ presents the largest delay in the stall conditions. Compared with the location of the LSB in the skin friction between the two values of the reduced frequency in Fig. 6(b), the effect on the skin friction due to the tip speed ratio in Fig.7(a) is minimal.

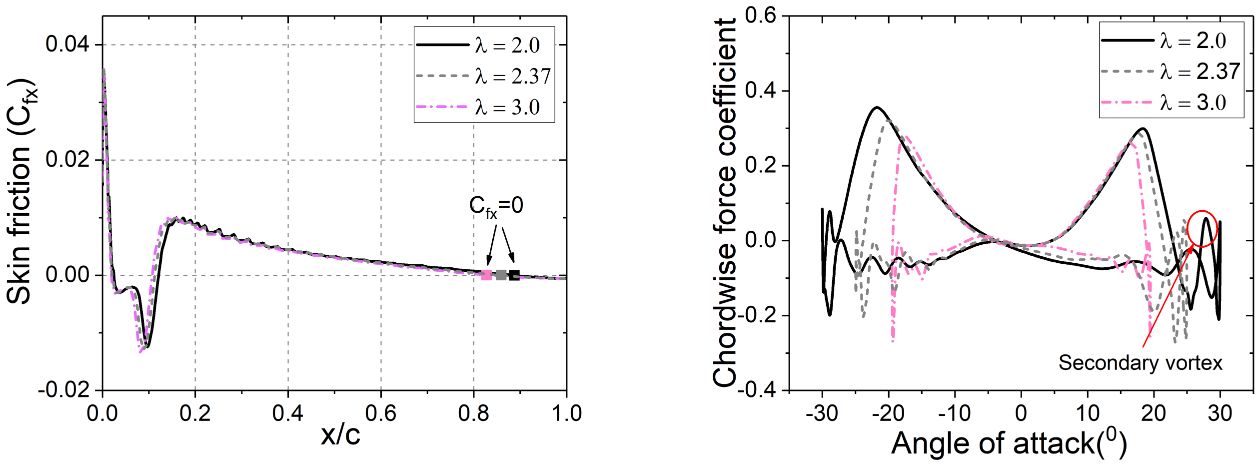

(a) (b)

Figure 7: (a) Skin friction, and (b) chordwise force coefficient, as a function of the angle of attack for λ= 3, 2.37 and 2 with values of $\kappa = 0.06$, $\beta = 0$ and $Re = 2 \times 10^5$.

The tip speed ratio plays a key role that is extremely important for the VAWT operation; it substantially influences the maximum angle of oscillation (α_{max}). Larger is the difference between the stall-onset and the maximum angle of oscillation, ($\alpha_{max} - \alpha_{os}$), then secondary vortices are more likely to occur and thus deeper stall conditions are observed.

For the tip speed ratio $\lambda = 2$, this difference, $\alpha_{max} - \alpha_{os}$, is 11.6°. This allows the release into the wake of the primary vortex formed at the leading edge (LEV), a shear layer vortex (that if formed at the TE, and is opposite in direction to the LEV) and the formation of a secondary vortex, as indicated in Fig. 8(a). The secondary vortex is also observed in the chordwise force coefficient, C_C, included in Fig. 7(b) where a second peak in C_c is identified.

In the case of $\lambda = 3$, the difference between α_{max} and α_{os} is 3.44° and hence, a primary vortex is released and the shear layer vortex is formed; there is no indication of a secondary vortex in the chordwise force coefficient in Fig. 7(b), neither in Fig. 8(b). More details on the deep stall conditions can be found in [32].

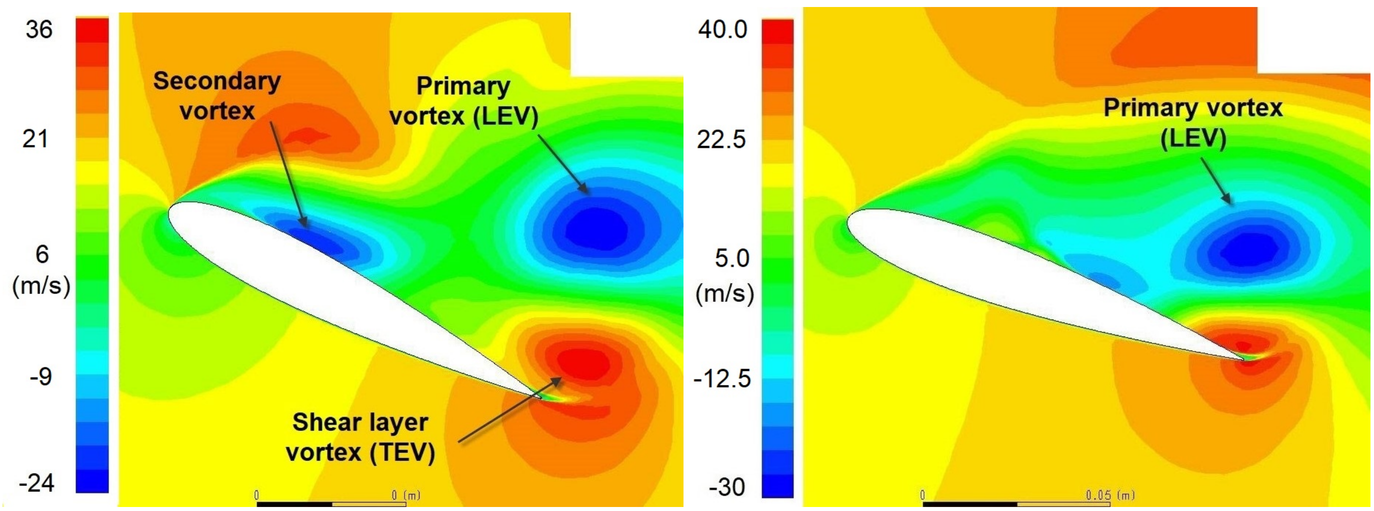

(a) (b)

Figure 8: The x-component velocity contour for the oscillating NACA0015 with (a) $\lambda = 2$ at $\alpha = 26.8°$, and (b) $\lambda = 3$ at $\alpha = 20°$ at $Re = 2 \times 10^5$.

(iii) The changes in the values of the pitch angle (β) produce an increase in the stall-onset angle if β increases the maximum angle of attack. For example, the stall-onset angle using $\beta = 10°$ was $\alpha_{os} = 17.25°$ and when using $\beta = -10°$ was $\alpha_{os} = 18.79°$. The corresponding maximum angle of attack (α_{max}) for both pitch angles was 20° for $\beta = 10°$ and α_{max}=40° for $\beta = -10°$. The maximum angle of attack, α_{max}, is calculated by performing a mathematical analysis of Eq.(1) that results in the expression $\alpha_{max} = \arctan([\lambda^2 - 1]^{-1/2}) - \beta$. Thus, the maximum angle of attack could be calculated using the corresponding pitch angle, a reduced frequency $\kappa = 0.06$ and, a tip speed ratio of $\lambda = 2$.

In Fig. 9(a), the skin friction for five values of β are plotted. It is observed that more positive is β thus closer is the laminar bubble to the leading edge and thus the stall occurs at a lower angle of attack. Additionally, the turbulent boundary layer point with $C_{fx} = 0$ has progressed closest to the LE for the most positive β value of 10° (Fig. 9(a)). Nevertheless, in general, the difference among the skin frictions curves for the range of pitch angles tested [-10° to 10°] are minimal and the overall variation in α_{os} due to the influence of the pitch angle (β) is less than 1.54°. The impact of the pitch angle on the stall-onset angle, compared with the tip speed ratio and the reduced frequency is the lowest.

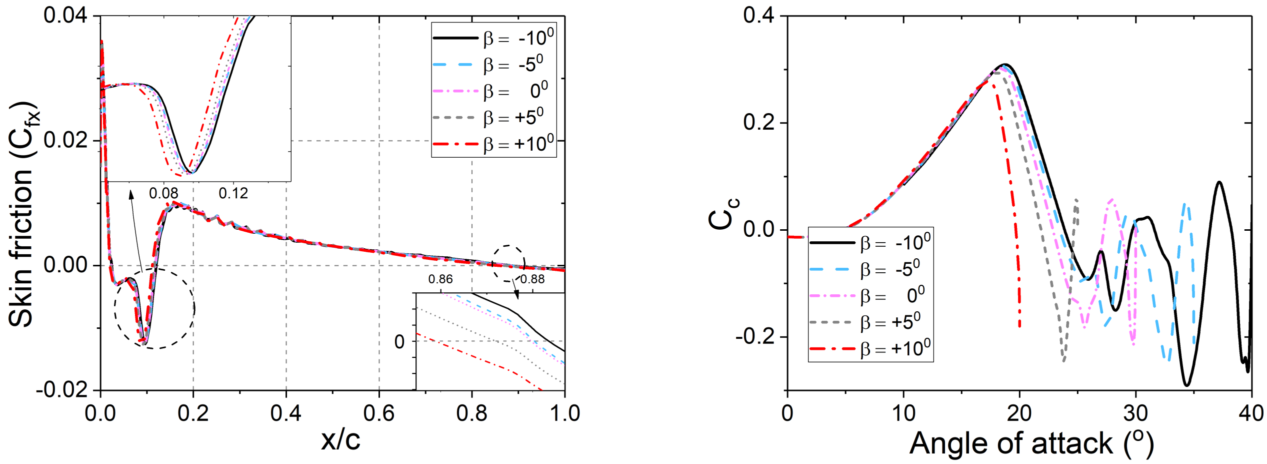

(a) (b)

Figure 9: (a) Skin friction along the non-dimensional chord length, and (b) chordwise force coefficient for several values of β at $Re = 2 \times 10^5$.

Similar to the tip speed ratio, the pitch angle also influences the maximum angle of attack. Thus, the severity in the stall conditions may be affected by changing the pitch angle. In Fig. 9(b) the chordwise force coefficient for the five values of β are plotted. With a more positive β value as explained in the previous paragraph, a slight decrease in α_{os} is observed but also a decrease in the maximum angle of oscillation. Thus, as observed in Fig. 9(b) for the most positive β value there is no indication of secondary vortices. On the contrary, with the most negative β value, despite experiences the larger stall-onset angle, it also produces a very large maximum angle of attack that causes two secondary peaks in the chordwise force as observed in Fig. 9(b). Those peaks in C_C indicate the formation of multiple secondary vortices and therefore, a largest severity in the stall conditions.

4.2. Non-dimensional pitch rate and Reynolds number effect

In this section, the stall-onset angle is evaluated as a function of the non-dimensional pitch rate, q, given by Eq. (3). This parameter involves the pitch rate, $\dot{\alpha}$, given by Eq. (2). Because $\dot{\alpha}$ is a time-dependent function, its value is evaluated at the instance when the angle of attack approaches the static stall angle. Three Reynolds number (based on the chord length) were evaluated by changing the magnitude of the incoming flow U_{ref} to 8, 20 and 33 m/s and obtaining the Reynolds number of 0.8, 2.0 and 3.3×10^5, respectively.

The analysis has revealed that the stall-onset angle, α_{os} increases linearly with the increase of the non-dimensional pitch rate, q, for all the Reynolds numbers tested, see Fig.10(a). Further, at the same q with the increase of the Reynolds number an increase in the stall-onset angle is observed.

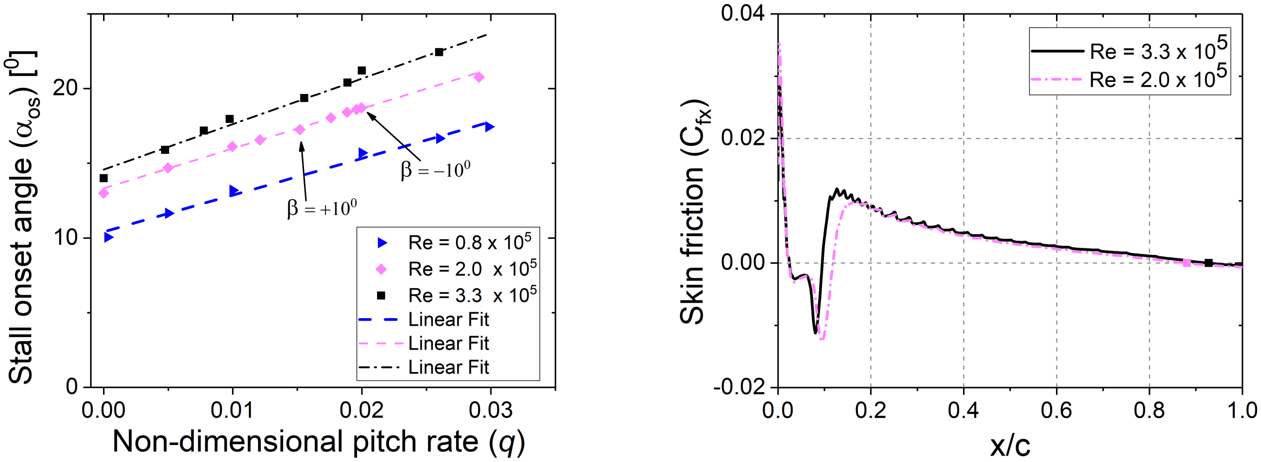

(a) (b)

Figure 10: (a) Stall-onset angle as a function of the non-dimensional pitch rate and Reynolds number for the NACA0015 aerofoil, and (b) Skin friction along the non-dimensional chord length for two Reynolds numbers at $\alpha = 13°$.

The increase in the dynamic stall-onset angle, α_{os}, due to the increase of the Reynolds number is consistent with the increase in the static stall angle that has been studied experimentally in several investigations [27]. The larger is the Reynolds number, the larger is the increase in the momentum exchange of the air particles from the outer boundary layer to the inner boundary layer of the aerofoil. Thus, improving the ability of the boundary layer to flow against the adverse pressure gradients and, as a consequence, longer is the time the boundary layer remains attached to the aerofoil surface.

The skin friction at the same angle of attack for two dynamic cases at two Reynolds number, Re, and with the same q are compared in Fig. 10(b). The region that encloses the air bubble, due to the laminar layer separation, is reduced at the highest Re as observed in Fig. 10(b) and the reattachment point as a turbulent boundary layer, occurs at an earlier distance from the leading edge of the aerofoil at Re= 3.3×10^5. Additionally, at the same angle of attack, the turbulent boundary layer depicts a more positive skin friction coefficient and the point where $C_{fx} = 0$ occurs later along the chord for

Re= 3.3×10^5. Thus, this indicated the boundary layer persists being attached at a larger angle of attack before separation occurs with an increase in the Reynolds number [59, 60].

Surprisingly, at the same Reynolds number, two dynamic simulations with different values of the tip speed ratio, reduced frequency and pitch angle that present similar values of non-dimensional pitch rate predict the stall-onset angles, α_{os}, with very similar values. For example, a simulation with tip speed ratio $\lambda = 2$, reduced frequency $\kappa = 0.09$ and pitch angle $\beta = -11°$ produces a stall-onset $\alpha_{os} = 18.37°$; for a second simulation with $\lambda = 1.5$, $\kappa = 0.075$ and $\beta = -13°$ the predicted α_{os} is 18.32°.

For the mentioned-above two cases with a similar non-dimensional pitch rate, the pressure coefficient peaks due to the laminar separation bubbles are very similar, as shown in Fig. 11(a). Further, for these same dynamic cases, their skin friction values with $C_{fx} = 0$ are encountered at similar locations along the chord, thus indicating laminar separation bubbles with the same size for both dynamic cases, see Fig. 11(b). Also, the turbulent boundary layer achieves $C_{fx} = 0$ at the same chord locations. Therefore, present results suggest the non-dimensional pitch rate value when approaches to the static stall angle is the most important parameter that defines the stall-onset angle in the VAWT motion. Therefore, the effect of the tip speed ratio, reduced frequency and pitch angle on the non-dimensional pitch rate (q) requires more attention when the stall-onset angle is being predicted in the VAWTs.

The positive effect of non-dimensional pitch rate, q, on the stall-onset angle has been supporting by analysing the simulations presented in Section 4.1. It has been observed that the reduced frequency (κ) in the dynamic simulations increases the non-dimensional pitch rate (q) from 0.018 to 0.029 for the reduced frequencies of $\kappa = 0.06$ and $\kappa = 0.09$ respectively. Thus, the stall-onset angle increases. In the case of the tip speed ratio (λ), the decrease in λ increases the q values: for $\lambda = 2$, 2.37 and 3, the values of q were 0.018, 0.016 and 0.0121 respectively, and the stall-onset angle decreases in value. Similarly, the pitch angle β that increases the q values increases the stall-onset angle, see Table 2. The increase in the stall-onset angle due to the increase of q due to the changes in the pitch angles are marked with arrows in Fig. 10 (a). Therefore, it is confirmed that anytime the operating parameters, individually or combined, increases the non-dimensional pitch rate, then, an increase in the stall-onset angle is also observed.

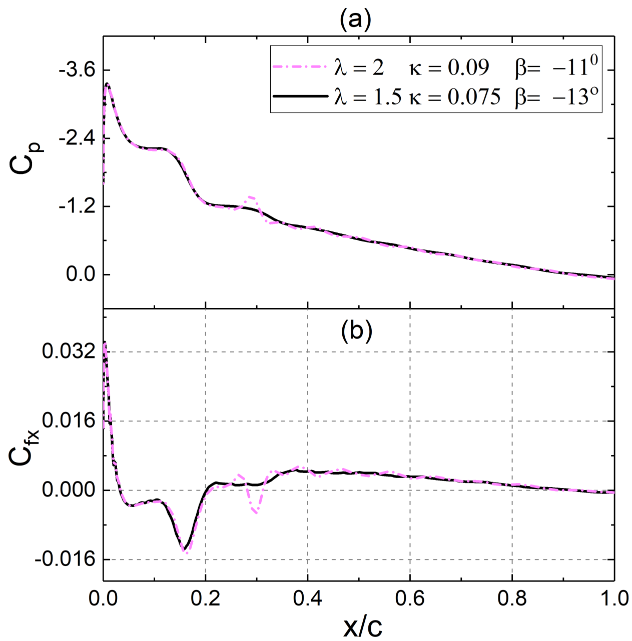

Figure 11: (a) Pressure coefficient and, (b) skin friction for two simulations with closed non-dimensional pitch rate value at $\alpha = 13°$.

Table 2: Pitch angle effects on the instantaneous non-dimensional pitch rate at α_{ss}.

β (°)	-10	-5	0	5	10
q	0.0199	0.0196	0.0188	0.0176	0.0152
α_{os} (°)	18.79	18.59	18.40	18.04	17.25
α_{max} (°)	40	35	30	25	20

4.3. Effect of the relative velocity on the stall-onset angle

In the previous sections, it was found that the stall-onset angle depends on the non-dimensional pitch rate and Reynolds number. In a VAWT with a constantly changing relative velocity, a fluctuation in both the non-dimensional pitch rate and Reynolds number occurs and this fluctuation increases in amplitude by decreasing the tip speed ratio. Therefore, the effect of the fluctuating relative velocity is investigated by using a time-varying incoming flow as given by Eq.(4) and described in the second approach in Section 2.

The fluctuation in the Reynolds number gives rise to the interest in investigating whether or not a difference on the stall-onset angle exists if using an average of the fluctuating relative velocity,

$V_{mean} \approx \lambda V_\infty$, instead of the actual fluctuating relative velocity. Two cases are being analysed using the fluctuating relative velocity described in Eq. (4). First, using a tip speed ratio $\lambda = 2$ and $V_\infty = 10$ m/s and, second, using a tip speed ratio $\lambda = 3$ and $V_\infty = 20/3$ m/s. For both cases, $\kappa = 0.06$ and $\beta = 0°$ were employed.

The analysis shows that the tip speed ratio $\lambda = 2$ produces a Reynolds number that fluctuates in the range $1 - 3 \times 10^5$ and $\lambda = 3$ produces Reynolds number in the range $1.4 - 2.6 \times 10^5$. These two cases with a fluctuating velocity maintain a similar average relative velocity, $\lambda V_\infty = 20$ m/s, thus resulting in the same average Reynolds number 2×10^5. In Table 3, the predicted stall-onset angle, α_{os}, for $\lambda = 2$ and 3, with a fluctuating velocity V_{rel} and a constant wind velocity V_{mean}, is presented. The stall-onset angle, α_{os} is included for the positive angles of attack (upstream zone of the rotor) and the negative angles of attack (downstream zone). In addition, the non-dimensional pitch rate (q) and the instantaneous velocity (V_{ins}) when the angle of attack approaches 13° are included for all the cases investigated in the upstream and downstream zones.

Table 3: Main characteristics of the stall onset for the two cases studied and evaluated upstream (up) and downstream (dw) of the rotor.

	Case (i) (λ=2)		Case (ii) (λ=3)	
Parameter	$V_{rel}(t)$	V_{mean}	$V_{rel}(t)$	V_{mean}
α_{os} (°) [upstream]	18.37	18.32	16.31	16.56
q [upstream]	0.013	0.0189	0.01	0.012
$V_{ins}(m/s)$ [upstream]	28.41	20.00	24.30	20.00
α_{os} (°) [downstream]	23.97	21.80	18.14	17.63
q [downstream]	0.096	0.050	0.027	0.020
$V_{ins}(m/s)$ [downstream]	10.55	20	14.57	20

For the case (i) with $\lambda = 2$, the stall-onset angle predicted using a fluctuating wind velocity results in $\alpha_{os} = 18.37°$ for the upstream zone of the rotor, and this is very similar to $\alpha_{os} = 18.32°$ when using the average wind velocity, V_{mean}. For all the cases, the non-dimensional pitch rate (q) and Reynolds number are evaluated at the instant the angle of attack is $\alpha = 13°$. [1].

[1] α_{ss} at Re=2×10^5 is 13°, despite the Reynolds number fluctuation can change α_{ss}, this fluctuation is very small,

For the incoming flow using the V_{rel} equation, the wind velocity calculated at $\alpha = 13°$ is $V_{inst} = 28.41$ m/s and $q = 0.013$; on the other hand, for the constant incoming wind velocity of 20 m/s case, the non-dimensional pitch rate is $q = 0.018$. Since q is larger for the constant wind velocity case, then it is expected to have a larger α_{os}, as explained in the previous section and illustrated in Fig. 10(a), but this is not observed because of the change in the Reynolds number. The Reynolds number has resulted in $Re = 2.8 \times 10^5$ for the incoming flow with the V_{rel} equation, and in contrast to the effect on q, the incoming flow with the constant wind velocity produces a $Re = 2 \times 10^5$ that is lower than the fluctuating velocity case.

For the case (ii) with $\lambda = 3$, similar results were obtained. The stall-onset angle α_{os} produced by both incoming flow conditions were very close in value; the calculated α_{os} with the fluctuating wind velocity was 16.31° and using a constant wind velocity, $\alpha_{os} = 16.56°$. The relative velocity again increases the actual wind velocity during the upstroke motion of the aerofoil, being $V_{ins} = 24.30$ m/s and q reduces its value to 0.01. Then, the increase in the Reynolds number, $Re = 2.4 \times 10^5$ increases α_{os}, see Table 3. On the other hand, the constant wind velocity produces $q = 0.012$ that is larger than in the V_{rel} of the incoming flow, but the Reynolds number is 2×10^5, slightly lower than the V_{rel} case; thus, both incoming flow conditions, the constant-average and the time-varying velocities predict similar stall-onset angles.

Present results suggest that for the upstream zone of the rotor, despite the fluctuations in both, the Reynolds number and the non-dimensional pitch rate (due to the relative velocity fluctuation), the use of average relative velocity, λV_∞ gives a good approach to the stall-onset angle.

Moreover, for the negative angles of attack (downstream zone of the VAWT rotor), and at a tip speed ratio of $\lambda = 2$, it is observed in Fig. 12 that the stall-onset angle, α_{os}, increases to 23.97° when using the V_{rel} as the incoming flow. This increase is due to the large increase in non-dimensional pitch rate, q, as a result of the very low wind speed V_{ins} of 10.55 m/s, see Table 3. Using the average relative velocity V_{mean}, the stall-onset angle was 21.80° and $q = 0.50$, and this non-dimensional pitch rate has half the value compared to that of the non-dimensional pitch rate when using V_{rel}.

This difference on the non-dimensional pitch rate and in the Reynolds number between the use of the V_{rel} incoming flow and the average value $V_\infty \lambda$ in the downstream region of the rotor is larger than

---

and the variation in q is negligible. See the influence of β on q in Section 4.2

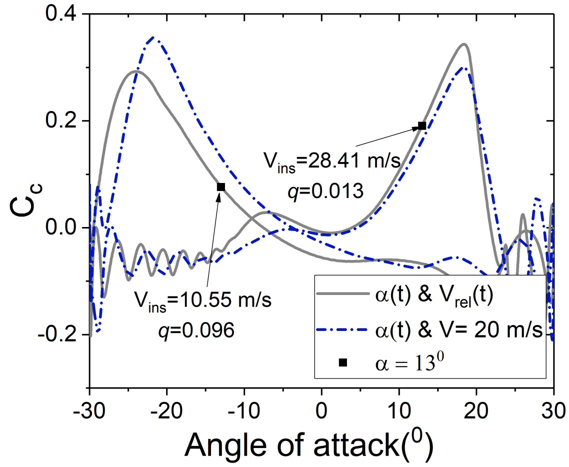

Figure 12: Chordwise force coefficient for $\lambda = 2$ using an incoming flow with: a constant velocity and with time-varying velocity given by the relative velocity Eq. (4).

in the upstream region of the rotor. Therefore, these findings suggest the use of an average relative velocity downstream is less convenient when evaluating the stall-onset angle in VAWTs.

Additionally, the computed chordwise force coefficients for the negative angles of attack, in Fig. 12, do not show a secondary peak after the stall-onset angle when compared with the constant velocity case of 20 m/s. The absence of a secondary C_C peak suggests that the dynamic stall phenomenon is less severe downstream than upstream due the higher values of the non-dimensional pitch rate $q = 0.093$. Thus, this explained why the vortex shedding in the experimental tests (in previous investigations) has been observed to be more frequent upstream of the VAWT rotor (positive angles of attack) than in the downstream of the rotor.

5. Discussion

The analysis of the operating parameters that affect the stall-onset angle in VAWTs carried out in the present investigation has revealed important findings for the applications in VAWTs and for the applications in dynamic stall algorithms.

The increase in the reduced frequency, κ, increases the stall-onset angle and delay the separation of the boundary layer to larger angles of attack. This delay in the separation of the boundary layer is in agreement with previous investigations on the reduced frequency that have used the ramp-up and sine-pitching motion and have focused mainly on the lift stall (L) rather than the stall-onset angle

[29, 39, 40]). The present findings explain why other authors that have studied the full rotor have found that an increment in the average reduced frequency ($c/2R$) may reduce the deep dynamic stall conditions to light stall or even non-stall at the same tip speed ratio [9].

The tip speed ratio and the pitch angle influence the magnitude of stall-onset angle. Nevertheless, their main role consists of defining the maximum angle of attack. When the maximum angle of attack is further increased to be larger than the stall-onset angle, deeper stall conditions are likely to occur. Hence, this means the several vortices formed upstream of the VAWT rotor can be released downstream and hence, reduce the power contribution of the VAWT in this latter zone. Thus, using the pitch angle as a strategy to control the maximum angle of attack can reduce the stalling degree conditions upstream of the rotor. Nevertheless, the tip speed ratio needs to be considered in order to select the most appropriate pitch angle, since both of them influence the maximum angle of attack and the stall-onset angle.

The pitch angle (β) evaluated here can be seen as being equivalent to the mean angle of oscillation from the sine-pitching motion. In previous investigations using the sine-pitching motions, instead of the VAWT angle of attack given by Eq. (1), a parameter called the equivalent reduced pitch rate has been proposed to evaluate the stall-onset angle [30, 47]. Nevertheless, in those studies an independence of the mean angle of oscillation with the stall-onset angle was suggested while in this paper, the pitch angle influences the stall-onset angle. Thus, the changes in the stall-onset with different β values explains why changing the pitch angle in the VAWTs blades changes the azimuthal angle where stall occurs and affects the severity of the stalling conditions [61].

The most interesting finding of this work is the influence of the typical parameters of VAWTs, namely, the tip speed ratio (λ), reduced frequency (κ) and pitch angle (β) on the investigated non-dimensional pitch rate (q) when the angle of attack approaches the static stall value. The larger is the non-dimensional pitch rate, then the larger is the stall-onset angle.

The positive effect of the non-dimensional pitch rate to delay the stall and calculated here using the VAWTs equations agrees with the effect of the non-dimensional pitch rate calculated with the ramp-up motion in some previous investigations. For example, using a ramp-up motion, the increase in the constant non-dimensional pitch rate produces an increase in the stall point (stall-onset or lift stall) [38, 39, 40, 44]. In addition, the non-dimensional pitch rate, as calculated for the sine-pitching motion in [31], has been shown to have a positive effect, namely increasing the stall-onset angle.

The confirmation of the equivalence among the non-dimensional pitch rates corresponding to the angle of attack of VAWTs, the sine-pitching and ramp-up motions are very important investigations that require much more exploration.

The increase in the stall-onset angle due to the increase in the Reynolds number observed in this paper using the VAWT angle of attack agrees with the results of the ramp-up tests performed by Choudhry et al. [39] where the lift-stall angle (L) as a function of the non-dimensional pitch rate was investigated at three Reynolds numbers.

The stall-onset angle as a function of the non-dimensional pitch rate, q, has not been well investigated at low Reynolds numbers, such as the requirement of VAWTs to operate at low wind speeds. Therefore, the obtained results for the stall-onset angle calculated in this paper, as a function of the non-dimensional pitch-rate at different Reynolds number, results in an essential tool in predicting the stall-onset angle for VAWTs. Also, this is very useful data that should be incorporated into the semi-empirical dynamic stall methods [35, 32, 30].

Semi-empirical dynamic stall methods use a time-delay constant that defines the linear relation of the stall-onset as a function of the non-dimensional pitch rate. This time delay constant depends on the Reynolds number and has been evaluated before mostly for Reynolds number as large as 1 million [62, 50, 63]. Therefore, the present results can be integrated into some of the dynamic stall models, such as the Leishman-Beddoes, to predict the unsteady loads in applications with a range of operation of the Reynolds number $0.8 - 3.3 \times 10^5$.

Overall, the present analysis has revealed that the combined effect of the tip speed ratio, reduced frequency and pitch angle on the non-dimensional pitch rate is an essential factor that dictates the level of delay in the stall conditions. Thus, this effect explain why it has been not possible in the previous studies to define a range of tip speed ratios where the dynamic stall occurs in VAWTs: the resulting non-dimensional pitch rate can increase or decrease according to the combined effect of the tip speed ratio, reduced frequency, pitch angle and relative velocity.

In VAWT analyses, it is very common to use the average of the fluctuating relative velocity to investigate its aerodynamics instead of using the actual fluctuating relative velocity. The findings of this paper have shown that in the upstream region of the rotor, the stall-onset angle is not significantly affected when an average the relative velocity, rather than the actual relative velocity is employed. In contrast, in the downstream region of the rotor, where the low magnitudes of the relative velocity produce high values of the non-dimensional pitch rate and low Reynolds numbers, the prediction of the stall-onset angle using an average of the relative velocity instead of the actual relative velocity may have a significant impact.

In this paper, a single blade using the angle of attack and relative velocity equations of a VAWT has been used to investigate the stall-onset angle. Although, these equations can be modified, by using the full rotor due to the number of blades or the curvature effects, the effect of the non-dimensional pitch rate and Reynolds number on the stall-onset angle are likely to still valid.

6. Conclusion

The investigations performed in this paper have revealed that the stall-onset angle in VAWTs is dominated by the combined effect of the tip speed ratio, reduced frequency, pitch angle and relative velocity on the two primordial parameters, the non-dimensional pitch rate (q) and the Reynolds number (Re), at the moment the angle of attack approaches the static-stall angle. The stall-onset angle increases with the increase in the non-dimensional pitch rate and with the increase in the Reynolds number. Therefore, techniques that can improve the non-dimensional pitch rate and Reynolds number can lead to a minimization of the dynamic stall effect on VAWTs. Moreover, the dynamic stall in VAWTs can take place at different azimuthal locations if the non-dimensional pitch rate and Reynolds number are affected by the changes in the tip speed ratio, pitch angle, reduced frequency and relative velocity during the VAWT operation.

The reduced frequency has been shown to have the most substantial influence in delaying the stall-onset to a larger angle of attack; this is followed by the tip speed ratio and then by the pitch angle. The last two parameters, i.e. the tip speed ratio and the pitch angle, are crucial in defining the maximum angle of oscillation and thus are the key to reducing the severity in the stalling conditions. Deep stall conditions and secondary vortices formation may be reduced if the difference in the maximum angle of attack and the stall-onset angle decreases.

The influence of the relative velocity on the stall-onset angle is attributed to its impact on the non-dimensional pitch rate and the Reynolds number. However, overall it produces similar stall-onset values in the upstream zone of the rotor than those values found using a constant average relative velocity. The relative velocities in the downstream zone of the rotor have lower magnitudes than in the upstream zone and, substantially higher values of the non-dimensional pitch rate than when using a constant-average relative velocity. Thus, the stall occurs at a larger angle of attack, and therefore the vortex shedding is less pronounced than in the upstream zone of the rotor.

It is important to note that although these results are based on one single aerofoil, the impact of the non-dimensional pitch rate and Reynolds number on the stall-onset angle in a full rotor is likely to be still valid since those are non-dimensional parameters and take into account any angle of attack and relative velocity history.

7. Acknowledgement

Nidiana Rosado Hau wishes to thank the National Council of Science and Technology (CONACYT) and the Secretary of Energy of Mexico (SENER) for the PhD funding.

References

[1] P. Delafin, T. Nishino, L. Wang, A. Kolios, Effect of the number of blades and solidity on the performance of a vertical axis wind turbine, Journal of Physics: Conference Series 753 (2016) 022033 (2016). doi:10.1088/1742-6596/753/2/022033.

[2] A. Bianchini, G. Ferrara, L. Ferrari, Design guidelines for H-Darrieus wind turbines: Optimization of the annual energy yield, Energy Conversion and Management 89 (2015) 690–707 (2015). doi:10.1016/j.enconman.2014.10.038.

[3] A. Dumitrache, F. Frunzulica, H. Dumitrescu, B. Suatean, Influences of some parameters on the performance of a small vertical axis wind turbine, Renewable Energy and Environmental Sustainability 1 (2016) 16 (2016). doi:10.1051/rees/2016024.

[4] A. R. Sengupta, A. Biswas, R. Gupta, Studies of some high solidity symmetrical and unsymmetrical blade H-Darrieus rotors with respect to starting characteristics, dynamic performances and flow physics in low wind streams, Renewable Energy 93 (2016) 536–547 (2016). doi:10.1016/j.renene.2016.03.029.

[5] A. Subramanian, S. A. Yogesh, H. Sivanandan, A. Giri, M. Vasudevan, V. Mugundhan, R. K. Velamati, Effect of airfoil and solidity on performance of small scale vertical

axis wind turbine using three dimensional CFD model, Energy 133 (2017) 179–190 (2017). doi:10.1016/j.energy.2017.05.118.

[6] Y. Guo, X. Li, L. Sun, Y. Gao, Z. Gao, L. Chen, Aerodynamic analysis of a step adjustment method for blade pitch of a VAWT, Journal of Wind Engineering and Industrial Aerodynamics (2019). doi:10.1016/j.jweia.2019.02.023.

[7] Q. Li, T. Maeda, Y. Kamada, J. Murata, K. Furukawa, M. Yamamoto, Effect of number of blades on aerodynamic forces on a straight-bladed Vertical Axis Wind Turbine, Energy 90 (2015) 784–795 (2015). doi:10.1016/j.energy.2015.07.115.

[8] M. Elkhoury, T. Kiwata, E. Aoun, Experimental and numerical investigation of a three-dimensional vertical-axis wind turbine with variable-pitch, Journal of Wind Engineering and Industrial Aerodynamics 139 (2015) 111–123 (2015). doi:10.1016/j.jweia.2015.01.004.

[9] A. Rezaeiha, H. Montazeri, B. Blocken, Characterization of aerodynamic performance of vertical axis wind turbines: Impact of operational parameters, Energy Conversion and Management 169 (February) (2018) 45–77 (2018). doi:10.1016/j.enconman.2018.05.042.

[10] R. Bravo, S. Tullis, S. Ziada, Performance testing of a small vertical-axis wind turbine, 21st Canadian Congress of Applied Mechanics CANCAM (September) (2007) 2–3 (2007).

[11] S. Brusca, R. Lanzafame, M. Messina, Design of a vertical-axis wind turbine: how the aspect ratio affects the turbine performance, International Journal of Energy and Environmental Engineering 5 (4) (2014) 333–340 (2014). doi:10.1007/s40095-014-0129-x.

[12] M. A. Miller, J. O. Dabiri, M. Hultmark, I. Brownstein, M. Lee, S. Duvvuri, Vertical-axis wind turbine experiments at full dynamic similarity, Journal of Fluid Mechanics 844 (2018) 707–720 (2018). doi:10.1017/jfm.2018.197.

[13] B. F. Blackwell, R. E. Sheldahl, L. V. Feltz, Wind Tunnel Performance Data for the Darrieus Wind Turbine with NACA 0012 Blades, Tech. Rep. May (1976).

[14] Q. Li, T. Maeda, Y. Kamada, J. Murata, K. Shimizu, T. Ogasawara, A. Nakai, T. Kasuya, Effect of solidity on aerodynamic forces around straight-bladed vertical axis wind turbine by

wind tunnel experiments (depending on number of blades), Renewable Energy 96 (2016) 928–939 (2016). doi:10.1016/j.renene.2016.05.054.

[15] N. Fujisawa, S. Shibuya, Observations of dynamic stall on turbine blades, Journal of Wind Engineering and Industrial Aerodynamics 89 (2) (2001) 201–214 (2001). doi:10.1016/S0167-6105(00)00062-3.

[16] G. Brochier, P. Fraunie, C. Beguier, I. Paraschivoiu, Water Channel Experiments of Dynamic Stall on Darrieus Wind Turbine Blades, Journal of Propulsion and Power Vol. 2 (No. 5) (1986) pp. 445 – 449 (1986).

[17] C. Simão Ferreira, G. Van Kuik, G. Van Bussel, F. Scarano, Visualization by PIV of dynamic stall on a vertical axis wind turbine, Experiments in Fluids 46 (1) (2009) 97–108 (2009). doi:10.1007/s00348-008-0543-z.

[18] P. Vittecoq, A. Laneville, The aerodynamic forces for a Darrieus rotor with straight blades: Wind tunnel measurements, Journal of Wind Engineering and Industrial Aerodynamics 15 (1-3) (1983) 381–388 (1983). doi:10.1016/0167-6105(83)90207-6.

[19] A. Laneville, P. Vittecoq, Dynamic Stall: The Case of the Vertical Axis Wind Turbine, Transactions of the ASME 108 (May 1986) (1986) 140–145 (1986). doi:10.1115/1.3268081.

[20] Q. Li, T. Maeda, Y. Kamada, Y. Hiromori, A. Nakai, T. Kasuya, Study on stall behavior of a straight-bladed vertical axis wind turbine with numerical and experimental investigations, Journal of Wind Engineering and Industrial Aerodynamics 164 (2017) 1 – 12 (2017).

[21] J. Edwards, L. A. Danao, R. J. Howell, PIV measurements and CFD simulation of the performance and flow physics and of a small-scale vertical axis wind turbine, Wind Energy 18 (2015) 201–217 (2015). doi:10.1002/we.1690.

[22] A.-J. Buchner, J. Soria, D. Honnery, A. J. Smits, Dynamic stall in vertical axis wind turbines: scaling and topological considerations, Journal of Fluid Mechanics 841 (2018) 746–766 (2018). doi:10.1017/jfm.2018.112.

[23] I. Paraschivoiu, Wind Turbine Design with empasis on Darrieus Concept, 4th Edition, Ecole Polytechnique de Montreal, Canada, 2002 (2002).

[24] F. Scheurich, R. E. Brown, Effect of Dynamic Stall on the Aerodynamics of Vertical-Axis Wind Turbines, AIAA Journal 49 (11) (2011) 2511–2521 (2011). doi:10.2514/1.j051060.

[25] P. A. Kozak, D. Vallverdú, D. Rempfer, Modeling vertical-axis wind-turbine performance: Blade-Element method versus finite volume approach, Journal of Propulsion and Power 32 (3) (2016) 592–601 (2016). doi:10.2514/1.B35550.

[26] J. Leishman, G. L. Crouse, State-space model for unsteady airfoil behavior and dynamic stall, in: 90th Structures, structural dynamics and materials Conferences. Mobile, Alabama, april 3-5, 1989, 1989, pp. 1372–1382 (1989). doi:10.2514/6.1989-1319.
URL http://dx.doi.org/10.2514/6.1989-1319

[27] G. B. Mccullough, D. E. Gault, Examples of Three Representative Types of Airfoil-section Stall at Low Speed. Technical Note 2502, Tech. rep., National Advisory Committee for Aeronautics (1951).

[28] A. Sharma, M. R. Visbal, Airfoil Thickness Effects on Dynamic Stall Onset, 23rd AIAA Computational Fluid Dynamics Conference (June) (2017). doi:10.2514/6.2017-3957.

[29] K. W. McAlister, L. W. Carr, M. W. J., Dynamic Stall Experiements on the NACA 0012 Airfoil (1978) 161 (1978). doi:10.1007/BF00575335.

[30] W. Sheng, R. A. Galbraith, F. N. Coton, Prediction of Dynamic Stall Onset for Oscillatory Low-Speed Airfoils, Journal of Fluids Engineering 130 (10) (2008) 101204 (2008). doi:10.1115/1.2969450.

[31] K. Mulleners, M. Raffel, The onset of dynamic stall revisited, Experiments in Fluids 52 (3) (2012) 779–793 (2012). doi:10.1007/s00348-011-1118-y.

[32] J. G. Leishman, T. S. Beddoes, A generalised model for airofoil unsteady aerodynamic behaviour and dynamic stall using the indicial method, in: 42nd Annual Forum of the American He copter Society, 1986, pp. 243–265 (1986).

[33] W. J. Mccroskey, L. W. Carr, K. W. Mcalister, Dynamic Stall Experiments on Oscillating Airfoils, AIAA Journal 14 (1) (1976) 57–63 (1976). doi:10.2514/3.61332.

[34] W. J. McCroskey, The Phenomenon of Dynamic Stall, Tech. rep., National Aeronautics and Space Administration (1981).

[35] F. J. Tarzanin, Prediction of control loads due to blade stall, 27th Annual National Forum of the American Helicopter Society (1971).

[36] J. W. Larsen, S. R. Nielsen, S. Krenk, Dynamic stall model for wind turbine airfoils, Journal of Fluids and Structures 23 (7) (2007) 959–982 (2007). doi:10.1016/j.jfluidstructs.2007.02.005.

[37] T. Lee, P. Gerontakos, Investigation of flow over an oscillating airfoil, Journal of Fluid Mechanics 512 (2004) (2004) 313–341 (2004). doi:10.1017/S0022112004009851.

[38] J. H. Strickland, G. Graham, Dynamic stall inception correlation for airfoils undergoing constant pitch rate motions, AIAA Journal 24 (4) (1985) 678–680 (1985). doi:10.2514/3.9325.

[39] A. Choudhry, R. Leknys, M. Arjomandi, R. Kelso, An insight into the dynamic stall lift characteristics, Experimental Thermal and Fluid Science 58 (2014) 188–208 (2014). doi:10.1016/j.expthermflusci.2014.07.006.

[40] J. Walker, H. Helin, D. Chou, Unsteady Surface Pressure Measurements on a Pitching Airfoil, in: AIAA Shear Flow Control Conference, Colorado, 1985 (1985).

[41] J. Strickland, G. Graham, Force coefficients for a NACA0015 airfoil undergoing constant pitch rate motions, AIAA Journal 25 (1987) 622–624 (1987).

[42] S. J. Schreck, W. E. Faller, M. C. Robinson, Unsteady separation processes and leading edge vortex precursors: Pitch rate and reynolds number influences, Journal of Aircraft 39 (5) (2002) 868–875 (2002).

[43] J. Walker, H. Helin, J. Strickland, An experimental investigation of an airfoil undergoing large-amplitude pitching motion, AIAA Journal 23 (8) (1985) 1142–1985 (1985).

[44] D. Daley, E. Jumper, Experimental investigation of dynamic stall for a pitching airfoil, AIAA Journal 21 (10) (1984) 831–832 (1984).

[45] W. J. Mccroskey, Unsteady Airfoils, Ann. Rev. Fluid Mech 14 (1982) 285–311 (1982).

[46] K. Lu, Y. H. Xie, D. Zhang, J. B. Lan, Numerical investigations into the asymmetric effects on the aerodynamic response of a pitching airfoil, Journal of Fluids and Structures 39 (2013) 76–86 (2013). doi:10.1016/j.jfluidstructs.2013.02.001.

[47] B. Rocchio, C. Chicchiero, M. V. Salvetti, S. Zanforlin, A simple model for deep dynamic stall conditions, Wind Energy (November 2019) (2020) 1–24 (2020). doi:10.1002/we.2463.

[48] O. Eboibi, L. A. M. Danao, R. J. Howell, Experimental investigation of the influence of solidity on the performance and flow field aerodynamics of vertical axis wind turbines at low Reynolds numbers, Renewable Energy 92 (2016) 474–483 (2016). doi:10.1016/j.renene.2016.02.028.

[49] J. McNaughton, F. Billard, A. Revell, Turbulence modelling of low Reynolds number flow effects around a vertical axis turbine at a range of tip-speed ratios, Journal of Fluids and Structures 47 (2014) 124–138 (2014). doi:10.1016/j.jfluidstructs.2013.12.014.

[50] E. Dyachuk, A. Goude, H. Bernhoff, Dynamic Stall Modeling for the Conditions of Vertical Axis Wind Turbines, AIAA Journal 52 (1) (2014) 72–81 (2014). doi:10.2514/1.J052633.

[51] W. Sheng, R. A. M. Galbraith, F. N. Coton, A New Stall-Onset Criterion for Low Speed Dynamic-Stall, Journal of Solar Energy Engineering 128 (4) (2006) 461 (2006). doi:10.1115/1.2346703.

[52] P. Ouro, T. Stoesser, L. Ramirez, Effect of blade cambering on dynamic stall in view of designing vertical axis turbines, Journal of Fluids Engineering 140 (June) (2018) 1–12 (2018). doi:10.1115/1.4039235.

[53] Y. Kim, Z.-T. Xie, Modelling the effect of freestream turbulence on dynamic stall of wind turbine blades, Computers & Fluids 129 (2016) 53–66 (2016). doi:10.1016/j.compfluid.2016.02.004.

[54] F. Geng, I. Kalkman, A. S. Suiker, B. Blocken, Sensitivity analysis of airfoil aerodynamics during pitching motion at a Reynolds number of 1.35×10^5, Journal of Wind Engineering and Industrial Aerodynamics 183 (November) (2018) 315–332 (2018). doi:10.1016/j.jweia.2018.11.009.

[55] J. A. Ekaterinaris, M. F. Platzer, Computational prediction of airfoil dynamic stall, Progress in Aerospace Sciences 33 (11-12) (1998) 759–846 (1998). doi:10.1016/S0376-0421(97)00012-2.

[56] A. S. Rezaei, H. Taha, Transition regime and its effects on the unsteady aerodynamic characteristics of a pitching airfoil, in: AIAA Scitech 2019 Forum, no. January, 2019, pp. 1–13 (2019).

[57] M. Ge, H. Zhang, Y. Wu, Y. Li, Effects of leading edge defects on aerodynamic performance of the S809 airfoil, Energy Conversion and Management 195 (April) (2019) 466–479 (2019). doi:10.1016/j.enconman.2019.05.026.

[58] D. M. Sharma, K. Poddar, Investigation of dynamic stall characteristics for flow past an oscillating airfoil at various reduced frequencies by simultaneous PIV and surface pressure measurements, 10th Internationnal symposium on particle image velocimetry -PIV13 (2013).

[59] I. H. Abbott, A. E. Von Doenhoff, Theory of Wing Sections: Including a Summary of Airfoil data, 1st Edition, New York, 1959 (1959).

[60] R. Gerakopulos, M. S. H. Boutilier, S. Yarusevych, Aerodynamic Characterization of a NACA 0018 Airfoil at Low Reynolds Numbers, 40th Fluid Dynamics Conference and Exhibit (July) (2010) 1–13 (2010).

[61] A. Rezaeiha, I. Kalkman, B. Blocken, Effect of pitch angle on power performance and aerodynamics of a vertical axis wind turbine, Applied Energy 197 (2017) 132–150 (2017). doi:10.1016/j.apenergy.2017.03.128.

[62] R. Carlson, R. Blackwell, G. Commerford, P. Mirick, Dynamic stall modelling and correlation with experimental data on airfoils and rotors, in: AHS/NACA-Ames Specialists Meeting on Rotorcraft Dynamics, 1974 (1974).

[63] M. Elgammi, T. Sant, A Modified Beddoes-Leishman Model for Unsteady Aerodynamic Blade Load Computations on Wind Turbine Blades, Journal of Solar Energy Engineering 138 (October 2016) (2016) 1–18 (2016). doi:10.1115/1.4034241.